Quantum efficiency calibration of opto-electronic detector by means of correlated photons method

Jianjun Li (李健军), Xiaobing Zheng (郑小兵), Yunjun Lu (卢云君), Peng Zou (邹 鹏), and Wei Zhang (张 伟)

Remote Sensing Laboratory, Anhui Institute of Optics and Fine Mechanics, Chinese Academy of Sciences, Hefei 230031

Received November 13, 2007

A new calibration method of detectors can be realized by using correlated photons generated in spontaneous parametric down-conversion (SPDC) effect of nonlinear crystal. An absolute calibration system of detector quantum efficiency is performed. And its principle and experimental setup are introduced. A continuous-wave (CW) ultraviolet (351 nm), diode-pumped, frequency-doubled, and solid-state laser is used to pump BBO crystal. The quantum efficiencies of the photomultiplier at 633, 702, and 789 nm are measured respectively. The coincidence peaks are observed using coincidence circuit. Some measurement factors including the filter bandwidth of trigger channel, the detector position alignment and polarization of the pump light are analyzed. The uncertainties of this calibration method are also analyzed, and the relative uncertainties of total calibration are less than 5.8%. The accuracy of this method could be improved in the future.

OCIS codes: 190.4410, 000.2190, 040.5160, 030.5630.
doi: 10.3788/COL20080607.0472.

In recent years, because of the requirements of quantitative remote sensing, radiometric calibration of sensors has become a fundamental technique in order to ensure the precision and availability of data in remote sensing. In traditional optical radiometry, primary standards are based on absolute sources or detectors. The common characteristics of those methods are in need to establish high-precision primary standards, and a chain of standard transfer[1−3]. They are exactly the factors that restrain the improvements of precision, and the transfer chain is a major source of uncertainty.

A new technique based on correlated photons obtained through parametric downconversion (PDC) was studied for the absolute calibration of photon-counting detectors[4−6]. The interest in this technique is the establishment of inherently absolute measurements at very low light levels, i.e., in the photon-counting regime. So far the reports about the method paid mainly attention to demonstrations and feasibility studies, much less emphasis was given to the systematic studies of uncertainty. The goal of this research is to provide some missing parts of this framework.

Wavelengths of correlated photons can be tuned over a significant portion of the visible and near-infrared spectrum when the phase matching angle is changed[7]. By means of this method, the quantum efficiencies of a photomultiplier at 633, 702, and 789 nm are systemically calibrated respectively.

The method of absolute calibration of photodetectors is based on the rigorous space and time coherence of photon in the PDC effect. For the process of parametric downconversion, a nonlinear uniaxial birefringent crystal is used. The crystal is aligned with its optic axis forming a large angle with the incident short-wavelength laser beam. A small fraction of the incident photon is spontaneously downconverted to pairs of photons satisfying the condition of energy and momentum conservation.

$$\omega_{\rm p} = \omega_{\rm s} + \omega_{\rm i}, \quad \vec{k}_{\rm p} = \vec{k}_{\rm s} + \vec{k}_{\rm i}, \tag{1}$$

where $\omega_{\rm p}$, $\omega_{\rm s}$ and $\omega_{\rm i}$ are pump, signal and idler frequencies, respectively. $\vec{k}_{\rm p}$, $\vec{k}_{\rm s}$ and $\vec{k}_{\rm i}$ are pump, signal and idler wave vectors, respectively.

If N is the total number of photon pairs emitted from the crystal in a given time interval. N_1, N_2 and $N_{\rm C}$ are the mean count rates recorded by signal detector, idler detector and in coincidence measurement, respectively, we have the following relationships[8]:

$$N_1 = \tau_{\rm Trigger}\eta_{\rm Trigger}N, \tag{2}$$

$$N_2 = \tau_{\rm DUT}\eta_{\rm DUT}N, \tag{3}$$

$$N_{\rm C} = \tau_{\rm Trigger}\tau_{\rm DUT}\eta_{\rm Trigger}\eta_{\rm DUT}N, \tag{4}$$

where $\eta_{\rm Trigger}$, $\eta_{\rm DUT}$ denote the quantum efficiency of signal and idler detectors, respectively. $\tau_{\rm Trigger}$, $\tau_{\rm DUT}$ denote the transmittance of signal and idler paths, respectively.

The quantum efficiencies of the two detectors are easily derived from Eqs. (2)—(4),

$$\eta_{\rm DUT} = \frac{1}{\tau_{\rm DUT}} \cdot \frac{N_{\rm C}}{N_1}, \tag{5}$$

$$\eta_{\rm Trigger} = \frac{1}{\tau_{\rm Trigger}} \cdot \frac{N_{\rm C}}{N_2}. \tag{6}$$

According to the principle above, we need to measure the coincidence count rates, trigger count rates and total optical losses of detector under test (DUT) path.

We set up a system to calibrate photomultiplier (PMT) in our laboratory. Figure 1 shows the schematic of optical setup. The diode-pumped, frequency-doubled Nd:vanadate laser (Coherent. Inc. Model Verdi V-18) provides a single-frequency green (532 nm) output, which is directed to Ti:sapphire laser (Coherent. Inc. Model MBR110) and then directed to frequency-doubled laser (Coherent. Inc. Model MBD200). A continuous-wave (CW) ultraviolet (UV) (351 nm) beam is produced. The

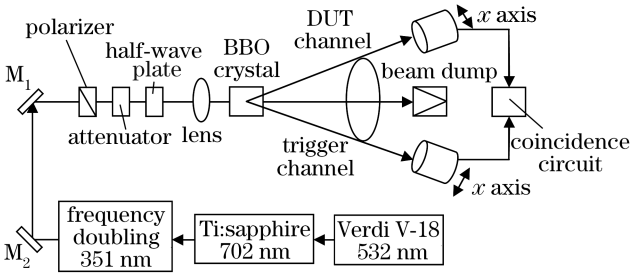

Fig. 1. Optical setup for determination of the quantum efficiency of the detector.

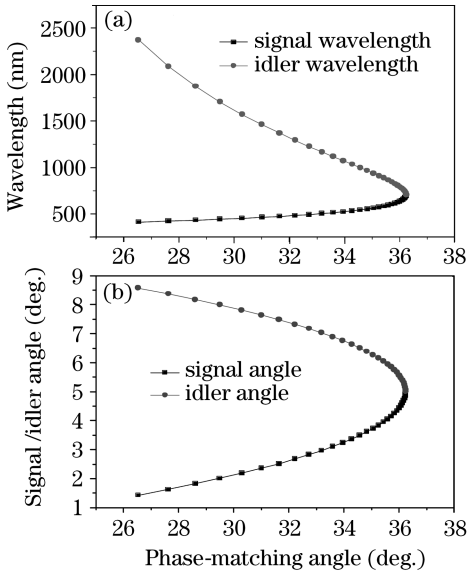

Fig. 2. Angle tune curve of BBO crystal. (a) Phase-matching angles versus wavelengths; (b) phase-matching angles versus emission directions.

351-nm beam is linearly polarized. A variable neutral-density filter is used to control the input power. The input to the crystal is typically 10 mW. Before entering the nonlinear crystal, the 351-nm beam passes through a zero-order, 351-nm half-wave plate, which allows to adjust the pump polarization to maximize the downconversion rate. A lens with a long focal length is used to increase the intensity of down-conversion correlated photon source. A beam diameter of 2 mm at the crystal is obtained. After passing through the crystal, the remaining, unscattered UV beam is directed to a beam dump. The crystal is cut for type-I phase-matching and oriented with its optic axis at 36.4° with respect to the pump beam. We measure the efficiencies by using two sets of conjugated photons. In the first set, both wavelengths are 702 nm. In the second set, the first wavelength at 633 nm and the second at 789 nm are obtained by orienting the crystal optic-axis at 36.16° from the pump direction. The crystal optic-axis should be rotated 0.24° from the degenerate case. The crystal input face is antireflection (AR) coated for the UV beam; the output face is broadband AR (BBAR) coated to reduce output losses over the range of 600 − 800 nm. By the phase-matching condition and Sellmeir equation of the crystal, signal and idler waves can be tuned over a wide range of wavelengths, and their emission directions are also changed, as shown in Figs. 2(a) and (b), respectively. As one can see, a wide range of spectrum of correlated photons, from the visible to the infrared, can be covered by appropriate choices of the phase-matching angle.

A small (6-mm diameter) iris at the position of 800 mm from the crystal is used to select the trigger photons. A large iris (12-mm diameter) at the position of 800 mm from the crystal is used to accept all the photons conjugate to those before the trigger detector. So the collection angles of trigger and DUT detector are 7.5 and 15 mrad respectively. In the two channels, different interference filters are put between the iris and detector. Detailed parameters of these filters are shown in Table 1.

Figure 3 shows the schematic of the electrical setup. The DUT detector is a Hamamatsu R2949 with a sensitive area of 7-mm diameter and dark counts below 300 counts/s. The trigger detector is a Hamamatsu R928 with a sensitive area of 8-mm diameter and dark counts below 500 counts/s. The output of each detector is amplified first by a fast charge-sensitive preamplifier. The typical pulse corresponding to a single-photon detection is of an amplitude of 80 mV, a rise time of 10 ns, and a full-width at half-maximum (FWHM) of 30 ns. The noise level is 40 mV. And then the pulse is directed into a constant-fraction discriminator (CFD). The discriminator threshold is set at −60 mV for most of the efficiency tests, as this is found to be sufficient for catching all the coincidence counts. The CFD output of the trigger channel is directed to a counter (yielding the trigger rate), and to the "start" input of a time-to-amplitude converter (TAC). The CFD output of the DUT channel is delayed (range from 1 to 63 ns) and sent to the "stop" input of the TAC. The TAC produces an output pulse with its height linearly proportional to time interval between the rising edges of the "start" and "stop" pulses. This pulse is simultaneously fed to multi-channel analyzer (MCA) and a single-channel analyzer (SCA). The MCA produces a time-correlated histogram with the amplitude of input pulses. The time-correlated photons produce a peak corresponding to the delay of setting; on the other hand, the uncorrelated photons produce a flat background. The

Table 1. Parameters of Interference Filters

Trigger Channel		DUT Channel	
λ_0 (nm)	Bandwidth (nm)	λ_0 (nm)	Bandwidth (nm)
792.14	9.22	633.40	9.10
702.77	9.53	702.81	9.53
632.92	2.96	792.14	9.22

λ_0: center wavelength.

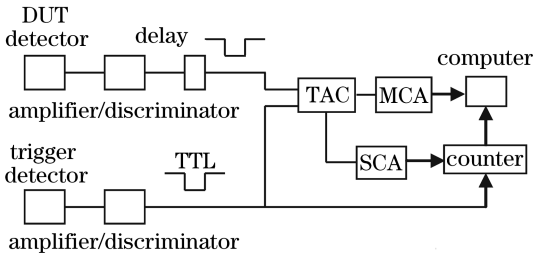

Fig. 3. Electrical setup for determination of the quantum efficiency of the detector.

SCA generates a standardized amplitude including a preselected voltage window. By setting the upper and lower thresholds of the voltage window in the SCA, we can obtain coincidence counts.

Previous experiments verified that the correlated photons emitted from our source were with a time correlation of better than 40 fs[9]. Thus, by observing the coincidence time profiles in our experiment, the temporal response of the detectors at the single-photon level can be tested. And the information of the production of correlated photons can be directly obtained from time-correlation profiles. Using the TAC and MCA, we obtained time-correlated profiles at 633, 789, and 702 nm respectively, and these wavelengths are referred to the trigger channel. The results are shown in Figs. 4(a)—(c), respectively.

For the above time-correlated profiles, we easily see a peak in the histogram generated by the MCA centered at this 25-ns time delay. Figure 4(a) displays the coincidence peak (FWHM, 1.1 ns) when the trigger channel has an interference filter peaking at 633 nm with a 3-nm FWHM. And we obtained that the ratio between the coincidence rate and accident coincidence rate per 100 s is about 100. Figure 4(b) displays the coincidence peak (FWHM, 1.3 ns) when the trigger channel has an interference filter peaking at 789 nm with a 10-nm FWHM. And we obtained that the ratio between the coincidence rate and accident coincidence rate per 100 s is about 40. Figure 4(c) displays the coincidence peak (FWHM, 1.4 ns) when the trigger channel has an interference filter peaking at 702 nm with a 10-nm FWHM. And we obtained that the ratio between the coincidence rate and accident coincidence rate per 100 s is about 10.

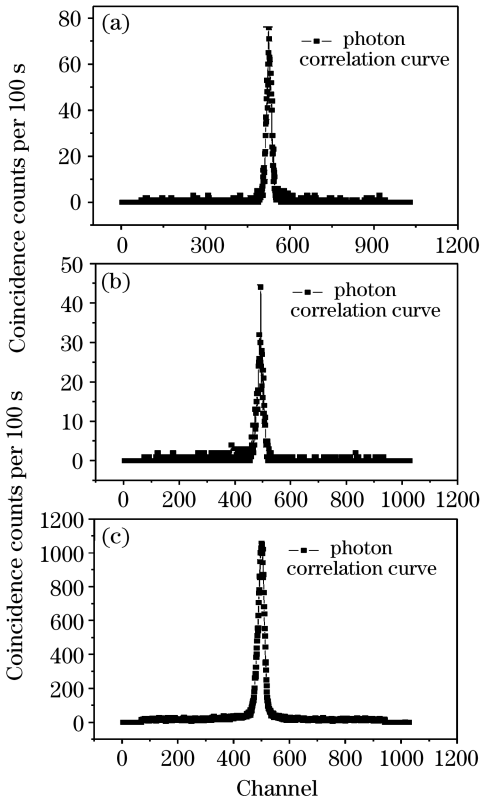

Fig. 4. Observation of coincidence time profiles when the trigger channel corresponds to different wavelengths of correlated photons. (a) 633-nm trigger; (b) 789-nm trigger; (c) 702-nm trigger.

It is easy to set the SCA window by observation of the coincidence peak. Usually we set the SCA window times beyond the FWHM of coincidence peak, where the SCA window is set at 5 ns, so the whole correlated photons can be received by the SCA. On the other hand, we calculate the ratio between the coincidence count rate and the accident coincidence count rate per 100 s. We can easily get the conclusion that the narrower the bandwidth (defined by the interference filter) of the trigger channel, the higher the ratio and smaller accident coincidence count rate.

The detector-alignment procedure is as follows. First, the trigger detector position is translated transversely (x axis in Fig. 1) across the cone of downconverted light to maximize the single-photon signal. This centers the detector on the central wavelength of the spectral interference filter. And then the DUT detector position also must be translated transversely (x axis in Fig. 1) across the cone of downconverted light to maximize the light correlated to the trigger.

A check of the trigger detector position must be performed by scanning horizontally to verify that the maximum correlated signal occurs at the maximum of the single trigger counts. Similarly, the DUT detector is needed to scan horizontally in order to maximize the coincidence counts. Figures 5(a) and (b) show the final results of the alignment procedure respectively when the PMT is calibrated at the wavelength of 702 nm.

In the trigger channel, the maximum counts are about 2.4×10^5 s^{-1}, and maximum coincidence counts are about 4.5×10^2 s^{-1} when the trigger detector is located at 6 mm, as shown in Fig. 5(a). Similarly we can see a flat coincidence counts when the trigger detector is located at the position around $4-6$ mm. So the emission angle of correlated photons is about 3.75 mrad.

In the DUT channel, the maximum coincidence counts

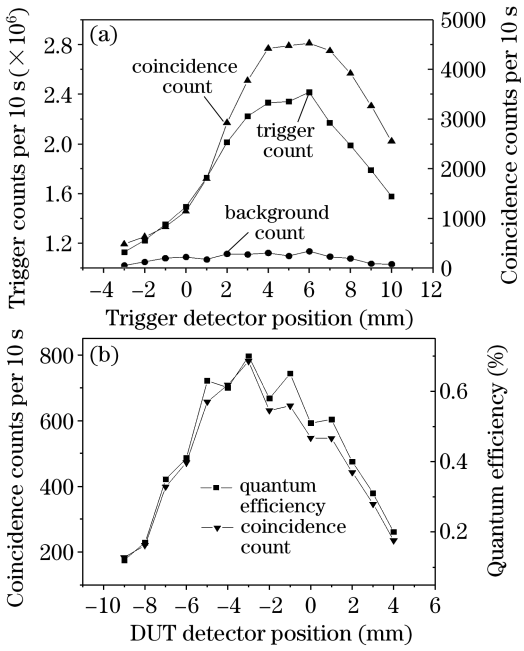

Fig. 5. Curve of detectors scanned transversely. (a) Trigger channel scanning; (b) DUT channel scanning.

are about $7.8\times10^2\ s^{-1}$, when the DUT detector is located at 3 mm, where the uncorrected DUT detector quantum efficiency is 0.80%, as shown in Fig. 5(b).

By using the similar detector-alignment procedure, the uncorrected DUT detector quantum efficiencies are 1.35% and 0.35% respectively when the PMT is calibrated at 633 and 789 nm respectively.

An important influence factor of correlated photons calibration is background counts[10]. It is mainly caused by scattered UV and laser fluorescence from both downconverted beam lines. By the phase-matching constraints, only one polarization orientation of the pump beam is to produce downconversion light. So we can turn off the creation of photon pairs by rotating the polarization of the pump beam by 90°. The advantage of this scheme is that, while the production of photon pairs is stopped, all other scattered light remains the same, allowing an excellent determination of the total scattered-light level. Figure 6 shows the trigger counts and the coincidence counts as the pump polarization is scanned whose minimum level is found to be 25% and 1.3% of the maximum respectively.

To calibrate the quantum efficiency of DUT detector, the background counts, dark counts of trigger channel, and accident coincidence counts should be considered. Additionally, the losses including the Fresnel reflection, the Fresnel transmittance of the crystal and the transmittance of the DUT interference filter are also considered. So Eq. (5) should be replaced by the following equation:

$$\eta_{\mathrm{DUT}} = \frac{1}{\tau_{\mathrm{DUT}}} \cdot \frac{N_{\mathrm{C}} - N_{\mathrm{AC}}}{N_1 - N_{\mathrm{B}}}, \tag{7}$$

where N_{AC}, N_{B} denote the accident coincidence counts and background counts of trigger channel, respectively.

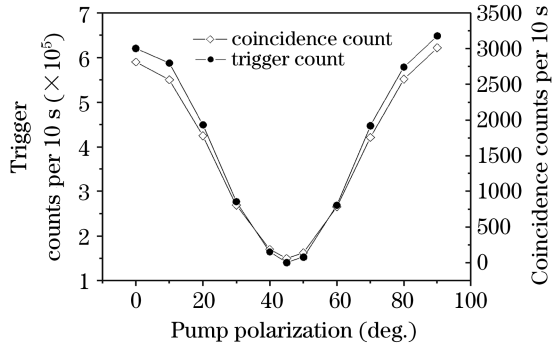

Fig. 6. Trigger counts and coincidence counts versus pump polarization.

Table 2. Relative Uncertainty Budget of Quantum Efficiency Measurement

Uncertainty Factors	Relative Uncertainty ($\times10^{-2}$)		
	633 nm	702 nm	789 nm
Trigger Optical Losses[12]	< 0.60	< 0.60	< 0.60
Trigger Counts	0.71	0.21	0.53
Trigger Background Counts	2.50	0.06	0.36
Coincidence Counts	5.17	2.97	4.04
Accident Coincidence Counts	0.15	0.24	0.56
Total Uncertainty	5.80	3.03	4.16

The statistical uncertainty is deduced by applying the uncertainty propagation law[11] to the model of measurements as described in Eq. (7). In Table 2, we report the relative uncertainty budget (coverage factor $k = 1$) of the quantum efficiency measurements, where each value is acquired 5 times over a period of 10 s.

In these results, the principal sources of errors come from the adjustments of the detectors on the light beams at selected wavelengths with narrow bandwidths.

Otherwise, the pump laser unsteady should be solved, which will influence the final calibration results. In the next step, we will insert a laser power controller in the pump light bench. Or we can increase the time of data accumulation to decrease the statistical fluctuation of the pump beam.

In summary, we implemented an experimental system of radiometric calibration based on correlated photons. Using the character of angle tuning of the nonlinear crystal, a photomultiplier working in the photon-counting regime is calibrated at 633, 702, and 789 nm, respectively. The uncertainties of measurement are less than 5.8%.

In comparison with traditional methods based on radiometric sources or detectors, the correlated photons technique has following advantageous. Firstly, it does not need a primary standard and a transfer chain. Secondly, it can easily select the calibration wavelengths based on the tune of crystal.

Our further research will focus on the reduction of the uncertainty of measurement. This intrinsically absolute calibration technique is independent of any other standards or transfer chain and is promising for radiometric calibration technique in the future.

This work was supported by the National Natural Science Foundation of China under Grant No. 60378027. J. Li's e-mail address is jjli@aiofm.ac.cn.

References

1. X. Zheng, H. Wu, J. Zhang, W. Zhou, Y. Liu, L. Wang, and Y. Qiao, Acta Opt. Sin. (in Chinese) **21,** 749 (2001).
2. Z. Lin, X. Zheng, L. Zhang, and J. Wang, Laser Optoelectron. Prog. (in Chinese) **44,** (4) 62 (2007).
3. J. Xing, S. Wang, and F. Li, Chinese J. Lasers (in Chinese) **33,** 509 (2006).
4. Y. Feng, X. Zheng, J. Li, and W. Zhang, Chin. Opt. Lett. **4,** 315 (2006).
5. Y. Feng, X. Zheng, W. Zhang, J. Li, and Y. Qiao, Acta Opt. Sin. (in Chinese) **27,** 457 (2007).
6. Y. Feng, X. Zheng, Y. Qiao, and J. Li, Chinese J. Lasers (in Chinese) **33,** (Suppl.) 200 (2006).
7. S. E. Harris, M. K. Oshman, and R. L. Byer, Phys. Rev. Lett. **18,** 732 (1967).
8. S. V. Polyakov and A. Migdall, Proc. SPIE **6583,** 65830A (2007).
9. D. C. Burnham and D. L. Weinberg, Phys. Rev. Lett. **25,** 84 (1970).
10. A. Migdall, S. Castelletto, I. P. Degiovanni, and M. L. Rastello, Appl. Opt. **41,** 2914 (2002).
11. B. N. Tayor and C. E. Kuyat, "Guidelines for evaluating and expressing the uncertainty of NIST measurement results" NIST Technical Note 1297 (1994 edn.).
12. L. Zhou and X. Zheng, Opto-Electron. Eng. (in Chinese) **33,** 32 (2006).